LAWRENCE
LIVERMORE
NATIONAL
LABORATORY

UCRL-JRNL-200816

A method for repairing amplitude defects in multilayer-coated EUV mask blanks

A. Barty, S. Hau-Riege, D. Stearns, M. Clift, P. Mirkarimi, E. Gullikson, H. Chapman, D. Sweeney

November 6, 2003

Applied Optics

A Method for Repairing Amplitude Defects in Multilayer-Coated EUV Mask Blanks

Anton Barty[1], Stefan Hau-Riege[1], Dan Stearns[2], Miles Clift[3], Paul Mirkarimi[1],
Eric Gullikson[4], Henry Chapman[1] and Don Sweeney[1]

[1] Lawrence Livermore National Laboratory, PO Box 808, Livermore, CA, 94550
[2] OS Associates, Los Altos, CA, 94024
[3] Sandia National Laboratories, Livermore, CA. 94550
[4] Lawrence Berkeley National Laboratories, Berkeley, CA, 94720

EUV mask blanks are fabricated by depositing a reflective Mo/Si multilayer film onto super-polished substrates. Localized defects in this thin film coating can significantly perturb the reflected field and produce errors in the printed image. Ideally one would want to manufacture defect-free mask blanks; however, this may be very difficult to achieve in practice. One practical way to increase the yield of mask blanks is to be able to repair a significant number of the defects in the multilayer coating. In this paper we present a method for repairing defects that are near the top surface of the coating; we call these amplitude defects because they predominantly attenuate the amplitude of the reflected field. Although the discussion is targeted to the application of manufacturing masks for EUV lithography, the conclusions and results are also applicable to understanding the optical effects of multilayer erosion, including ion-induced multilayer erosion and condenser erosion in EUVL steppers.

1 Introduction

EUV mask blanks are fabricated by depositing a reflective Mo/Si multilayer film onto super-polished substrates. Localised defects in this thin film coating can significantly alter the reflected field and introduce errors in the printed image. Ideally one would want to produce defect-free mask blanks; however, this may be very difficult to achieve in practice. An alternative way to increase the yield of mask blanks is to repair multilayer defects, and to this effect we have developed two complementary defect repair strategies for use on multilayer-coated EUVL mask blanks.

A defect is any area on the mask that causes unwanted variations in EUV dose in the aerial image obtained in a printing tool, and defect repair is correspondingly defined as any strategy that renders a defect unprintable during exposure. The term defect mitigation can be adopted to describe any strategy that renders a critical defect non-critical when printed.

In reflective EUV masks defects can occur in both the reflective mask substrate and the patterned absorber layer. Defects in the patterned absorber layer consist of regions where metal, typically chrome, is unintentionally added or removed from the pattern leading to errors in the reflected field. There currently exist technologies based on ion beam milling and ion beam assisted deposition for repairing defects in the absorber layer of transmission lithography masks, and it is reasonable to expect that these this technology will be extended to the repair of absorber defects in EUVL masks[1]. However, techniques designed for the repair of absorber layers can not be directly applied to the repair of defects in the mask blank, and in particular the multilayer film. A problem unique to EUVL is the existence of defects in the reflective multilayer coating applied to mask blanks prior to patterning.

A typical EUV multilayer coating consists of between 40 and 80 alternating bilayer pairs of molybdenum and silicon with each bilayer consisting of approximately 3nm thickness of molybdenum and approximately 4nm thickness of amorphous silicon. The reflectivity of the multilayer is a resonant property of the alternating layer structure and is at an optimum when all the layers interfere constructively. Because reflection takes place throughout the bulk of the multilayer any deformation or disruption of the layer structure can manifest itself as a defect. The goal in mask blank manufacture is to produce defect-free mask blanks, however this may be difficult to achieve in practice due to defects introduced during the coating process. The key question for mask blank manufacture and mask blank cost is maximisation of the yield of useable mask blanks. Trends in mask manufacturing technology suggest that there is a cost benefit in developing viable techniques to repair defects in the mask blank; the greater the number of defects that can be successfully addressed using multilayer repair, the greater the yield of useable mask blanks for a given process defect level reducing the cost of individual mask blanks.

A technique has recently been described for the repair of defects nucleated near the base of the multilayer structure, which primarily affect the phase of the reflected field[2,3,4]. In order to maximise the probability of being able to repair a defect it is desirable to have repair strategies that can address defects occurring on the substrate and/or mask blank surface as well as defects introduced during multilayer deposition. In this paper we present a technique for repairing defects located in the top layers of the multilayer coating; we call these amplitude defects because they predominantly attenuate the amplitude of the reflected field, and they are typically introduced either during deposition of the top layers of the multilayer stack or subsequent to multilayer deposition. We also describe how the complementary techniques of amplitude and

phase defect repair can be combined to address defects occurring through the entire multilayer stack, including defects located on the surface and at the substrate.

1 Amplitude defect repair method

Defects located in the upper layers of the multilayer stack can affect the multilayer reflectivity in one of two ways:

(a) if the particle is opaque the incident field does not penetrate the defect and the amplitude of the reflected field is directly reduced; or

(a) the particle can damage the multilayer structure in its vicinity, either during the embedding process or by perturbing the subsequent multilayer growth, reducing the multilayer reflectivity which in turn decreases the amplitude of the reflected field. Even if the particle does not remain embedded in the coating the damage caused to the multilayer structure itself can act as an amplitude defect because the multilayer structure has been damaged in the region where the particle was located.

In both cases the amplitude of the reflected field is reduced in the vicinity of the defect. The basic principle of the amplitude repair method is to restore the local reflectivity by removing the particle and any damaged regions of the multilayer coating. This process leaves behind a shallow crater in the multilayer, but if done in a properly controlled manner the reflectivity of the repaired region can be restored to nearly defect-free levels and the effect of the defect on the printed image thereby mitigated.

To successfully repair a lithographic mask there must not be a significant variation in contrast in the bright-field intensity of a lithographic image across the repaired area after repair,

which in turn places constraints on the repair technique. In particular, the requirement of no significant contrast variation means that:

(a) a sufficient number of multilayers must remain after repair for the reflectivity degradation to be negligible,

(a) the underlying layers of the multilayer stack remain undamaged so that they can still reflect EUV light;

(a) there is no deposition of particles elsewhere on the mask blank resulting from the milling process; and

(a) any phase shift introduced into the reflected field by milling out a small region of the reflective surface be sufficiently small that the phase structure of the crater does not itself introduce a defect into the printed image;

The first and last constraints, (a) and (d), represent theoretical limitations on the size and shape of the repair region with (a) determining the maximum repair depth and (d) determining the required lateral extent of the repair zone, which in turn determine the size and location of defects that can be repaired using this technique. Constraints, (b) and (c), represent practical considerations dependent on experimental implementation.

One way of achieving this is by physically removing the particle using a focussed ion beam as shown in Figure 1.

1.1 Controlling reflectivity loss due to layer removal

The reflectivity of a multilayer is a direct function of the number and structure of bilayers in the multilayer stack. An EUV mask blank may have between 40 and 80 bilayer pairs in the multilayer stack, with the reflectivity of the Mo/Si multilayer at 13.5nm attaining approximately

98% of the maximum possible reflectivity by the time the coating is 40 bilayers thick. The decrease in reflectivity with layer removal imposes a practical limitation on the depth of defect that can be removed using bilayer removal as sufficient layers must remain for the reflectivity in the repaired region. Thus removing up to 40 bilayers from a multilayer originally 80-bilayer thick should decrease the intensity of the reflected field by less than 1% due to layer removal alone, whilst for a 50-bilayer multilayer only 10 bilayers may be removed for the intensity of the reflected field to decrease by the same amount.

The process of milling the repair region will not necessarily remove an integral number of bilayers across the entire repaired region, thus it is necessary to consider the effect of removing a fractional number of bilayers. The reflectivity of a multilayer as a function of thickness removed is plotted in Figure 3 for a Mo/Si multilayer of 80 bilayers initial thickness; note the initial increase in reflectivity as the native SiO_2 oxide layer is removed, and the subsequent oscillation in reflectivity as alternate layers of Mo and Si are exposed as the uppermost layer. Note that the overall reflectivity drop is negligible provided more than 40 bi-layers remain after repair as expected, but there remains a 1% modulation in reflectivity due to the alternating bands of Mo and Si as top layers of the multilayer stack.

1.2 Controlling phase errors in the repaired region

Milling away layers of the multilayer stack will introduce a phase shift into the reflected field, and it is therefore essential that the crater profile be carefully controlled so as to minimise printability of the repaired region in a lithographic tool. To assess the effect of phase variations, consider a feature on the mask that only affects the phase of the reflected light. The complex transmission of this object can be described as:

$$\Box(\vec{r}) = e^{2\Box\Box(\vec{r})/\Box}$$

where $p(\vec{r})$ is the optical path difference (OPD) introduced into the reflected light by the feature. Although the object is transparent, the phase structure nevertheless modifies the energy flow of the reflected light, which in turn introduces variations in the aerial image intensity. For objects that are considerably larger than the point spread function of the imaging optic, the diffracted intensity remains within the entrance pupil of the optic and no light is lost from the system. If the camera is aberration free this diffracted light will be redirected to an image of uniform intensity; however, if there are aberrations in the optical system the diffracted intensity will not recombine with the correct phase to give uniform intensity, resulting in intensity variations in the image plane that depend on the aberration structure of the optic. The dominant aberration term in a high-quality lithographic optic is defocus, and it is well known that defocus gives phase-contrast imaging[5]. For objects larger than the image resolution, the image intensity of the object $\Box(\vec{r})$ is given by[6]:

$$I(\vec{r}) = 1 + \frac{\Box z}{k}\Box^2\Box(\vec{r})$$

where $\Box z$ is the defocus distance at the mask and $k = 2\Box/\Box$. From this relation it can be seen that the intensity distribution varies linearly with defocus and with the second derivative of the OPD, and that contrast is reversed on either side of best focus. A linear phase slope is equivalent to a tilt on the mask, resulting in a lateral shift of the intensity but no intensity contrast.

Multilayer reflection occurs throughout the multilayer bulk rather than from the surface, and layer removal does not alter the relative position of layers within the stack. After a crater is formed the underlying layer structure forces all waves to be in phase with respect to each other within the multilayer itself, thus the phase of the reflected field in the repair region does not simply follow the surface profile. The only contribution to phase error occurs from the refractive index difference between the vacuum inside the crater and the multilayer bulk. The refractive

index of the multilayer is equal to the ratio of the wavelength of light in vacuum (λ) to that in the multilayer, which for a multilayer of normal incidence is equal to twice the bilayer period. For a typical EUVL Mo/Si multilayer we have $\lambda = 13.43nm$ and $2d = 13.80nm$ giving $1 - n = 0.03$. That is to say that the refractive index of the multilayer is very nearly the same as for vacuum, thus the phase shift for a given crater depth is just 0.03 times the profile of the crater itself[7]. The optical path difference (OPD) for light reflected from a Gaussian-shaped crater on the mask of maximum depth h is the maximum depth of the crater and 1/e radius of σ is therefore of the form

$$p(\bar{r}) = 2(n-1)he^{-r^2/\sigma^2}$$

where n is the average refractive index of the multilayer as described above. The intensity change through focus is related to the second derivative of the phase; for the Gaussian-shaped crater described above the second derivative has the form:

$$\nabla^2\left(e^{-\bar{r}^2/\sigma^2}\right) = \frac{-2\left(\sigma^2 - r^2\right)}{\sigma^4}e^{-r^2/\sigma^2}$$

with extrema of $-2/\sigma^2$ at $r = 0$ and $4e^{-3/2}/w^2 = 0.89/w^2$ at $r = \pm\sqrt{3/2}\sigma$. The range of intensity variation in the printed image can be computed directly from the extrema of the second derivative of the crater profile, and is given by

$$I_i = 1 + 2(1-n)\frac{\Delta z}{k}\sigma m_i/\sigma^2$$

where m_1 is equal to $m_{\min} = -2$ or $m_{\max} = 0.89$ respectively for the minimum and maximum intensities. For defect repair craters we have $2(1-n)\Delta z\, h/\sigma^2 << 1$, so the image contrast, defined as

$$C = \frac{I_{\max} - I_{\min}}{I_{\max} + I_{\min}}$$

can be approximated by

$$C \approx \frac{2(1-n)|\Delta z|h}{\lambda^2}\left|\frac{m_{\max}-m_{\min}}{2}\right|$$

The contrast variation induced by the repair zone increases with defocus distance, so that the maximum contrast variation occurs at the maximum value of defocus within the process window of printing. The maximum defocus is no larger than the depth of focus, which is in turn defined by the numerical aperture (NA) of the imaging system and is given by $\pm\lambda/2NA^2$, where NA in this case is the NA facing the mask. The depth of the crater can be characterised in terms of the number of bi-layers removed, N, as $h = 2dN = \lambda N/n$. The maximum contrast $C_{\max}$ within the process window of the lithographic tool can therefore be expressed as

$$C_{\max} = 1.45\frac{(1-n)N}{n(\lambda/\Delta)^2}$$

where $\Delta = \lambda/2NA$ is the spatial resolution at the mask. *We therefore see that larger diameter craters with gently sloping sides will not print as easily as smaller craters with steep sides*. For example, for the removal of 20 bilayers from a Mo/Si multilayer mask we have $C_{min}=0.89\Delta^2/\lambda^2$, and to ensure that the contrast induced by the repair is less than 1% we must have $\Delta>9.45\lambda$.

For a 0.25NA 4x stepper system operating at 13.5nm the NA facing the mask is 0.0625NA and the spatial resolution on the mask is $\Delta = 107nm$, thus a 20 bilayer (130nm) deep repair site must be 2μm or more in diameter to ensure that the repaired region does not manifest itself as a phase defect in the printed image. The dependence of aerial image contrast on repair site depth and diameter for a Gaussian shaped repair site profile is shown in Figure 2: panel (a) shows contrast as a function of depth and diameter, whilst panel (b) shows the minimum repair diameter required to achieve a given contrast level for various repair depths. The minimum repair zone

diameter can be seen to be a function of repair depth, with deeper repair sites requiring larger diameter repair zones to ensure an acceptably low variation in the aerial image contrast.

1.3 Image placement error and depth of focus

Within the repair region the mask surface is slightly lower than in surrounding regions, thus the absorber pattern is at a different depth with respect to unrepaired regions of the mask, resulting in a small amount of image placement error. The mask is illuminated by EUV light at an angle of 6° to the normal, thus placing absorber features at different depths leads to some image placement error in the printed image as illustrated in Figure 4. The magnitude of the image placememt error Δx in the wafer plane can be determined from the geometric image shift and is given by

$$\Delta x = Md\tan\theta$$

where d is the crater depth, θ is the angle of illumination and M is the magnification of the projection optics. For a typical 0.25NA EUV projection optics we expect the angle of incidence to be approximately 6° ($\theta \approx 6°$) and the reduction ratio to be a factor of 4 ($M = 0.25$), Image placement error calculated for absorber features positioned within the crater at different depths are listed in Table 1:

Depth of repair site (Number of bi-layers)	Depth of repair site (d, nm)	Worst-case image placement error $(\Delta x, nm)$
2	13.8 nm	0.36nm
5	35 nm	0.9nm
10	69 nm	1.8nm
15	104nm	2.7nm
20	138nm	3.6nm
40	276nm	7.2nm

Table 1

Inspection of Table 1 shows that the image placement error caused by the absorber being at a different depth within the repair site is comfortably within the allowed overlay budget of 15nm allowed at the 45nm node. This is the image placement error at the worst place in the repair site, which itself is only microns in size, thus the added contribution to the overall overlay budget is both small in magnitude and occurs only in a small micron-sized region of the entire mask.

Note also that the anticipated depth of the repair region is well within the depth of focus of the projection optics. The depth of focus of an optical system is approximately

$$DOF \approx \pm \frac{\lambda}{2(NA)^2}$$

Thus for a typical 0.25NA, 4x reduction projection system the NA facing the mask will be 0.0625NA, giving a depth of focus at the mask of approximately $\pm 1.7\mu m$. This is much greater than the anticipated depth of the repair region, thus we do not anticipate any detrimental effects due to additional defocus caused by the absorber layer being placed at a different depth within the repair region, which itself is only a small micron-sized region of the entire mask.

1.4 Aerial image modelling

We also performed aerial image modelling to assess the effect of amplitude repair on the printed lithographic image. In the example presented here we placed a 100% opaque, 140nm defect on the mask was placed in proximity to a 35nm (at the wafer) isolated line and calculated the aerial image for a 0.25NA, 4x reduction imaging system with partial coherence $\sigma = 0.7$. The corresponding lithographic image was computed using a threshold resist at 30%, this being the threshold which prints the defect-free line to 35nm in best focus. Without amplitude repair and with the defect placed at the worst position with respect to the line this defect leads to a 100% CD change, as shown on the left in Figure 5.

Next we consider the case where the defect has been removed using our repair method, but there remains some variation in reflectivity across the repaired region. For a reflectivity drop of 3.5% the aerial image after repair is shown on the right in Figure 5: in the repaired region the change in CD within the repair site is approximately 2.5%. This change in CD is directly related to the reflectivity variation inside the crater and can be calculated for a range of reflectivity drops, giving the plot shown in Figure 6. As expected the CD change in the printed image is directly related to the reflectivity drop in the repaired region, motivating the search for a practical repair process that minimises reflectivity variation within the repaired region. This aerial image modelling also confirms that that amplitude repair technique is capable of significantly mitigating the effect of repairable amplitude defects on the printed lithographic image, and can turn critical defects into small non-critical variations in CD within the repair region of a few microns in diameter.

1.5 Constraints on defects repairable using amplitude repair

The maximum defect depth able to be repaired using the amplitude (ion beam) technique depends on two factors: sufficient bilayers must remain after repair for the local reflectivity to be not significantly harmed, and the defect must be close enough to the surface so that repair will not introduce an unacceptable amount of image placement error. From Figure 3 it is apparent that layer removal does not adversely harm the multilayer reflectivity provided that more than 35 bi-layer remain in the multilayer stack after repair. Turning to the question of image placement, from Table 1 we see that provided the craters can be made of arbitrary profile the removal of up to 280 nm of multilayer (equivalent to 40 bilayers) introduces less than 7.6nm of image placement error at the worst position in the repair site. The image placement budget is 15nm at the 45nm node, thus it is feasible to remove 40 bi-layers whilst remaining within the overlay

budget at this technology node. One further constraint is that the profile of the repair region must be made sufficiently gentle that the repair region does not become an amplitude defect; whilst this requirement affects the shape of the repair region and does not impose an additional constraint on the depth of defect that can be repaired. The selection of appropriate limiting values is subject to some discretion, but we suggest that it is possible to remove a defect using amplitude repair provided that no more than 20 bilayers are removed, so as to preserve image placement, whilst more than 35 bi-layers must remain under the repair region to preserve reflectivity.

2 Experimental progress

To demonstrate the amplitude-defect-repair technique applied the amplitude defect repair technique to a Mo/Si EUV multilayer of the type used in mask blank manufacture. The particular multilayer used consisted of 50 bilayers of Mo/Si bilayers deposited on a silicon wafer substrate using an ion-beam deposition system, with a reflectance of 66% at 13.4nm after deposition. Amplitude repair sites of up to 5 bilayers-deep craters were formed in the multilayer using a 500eV argon ion beam as shown in Figure 8(a). To minimise the reflectivity loss due to ion milling we formed the craters with the ion beam at an angle of 65 degrees off-normal so as to minimise the penetration of ions into the multilayer. The Ar ion beam was about 150□m in diameter and was scanned to mill craters that were rectangular-shaped and approximately 4x17mm^2 in size. The craters were substantially larger that the craters suggested for amplitude-defect repair to allow for EUV reflectance measurements using the scanning reflectometer beamline at the Advanced Light Source (ALS) at Lawrence Berkeley Laboratory. Figure 8(c) shows an optical microscope image of a crater formed by argon sputter-etching.

To minimize oxidation in the repair region a capping layer was deposited over the repair site using in-situ ion beam sputtering. Without breaking the vacuum and exposing the crater to atmosphere, a capping layer was deposited by directing a 1000eV argon-ion beam at a sputter target held in proximity to the repair region as shown in Figure 8(b). By locating the target close to one edge of the crater the capping layer thickness varied continuously along the length of the crater depending on the proximity to the sputter target. Several candidate capping layer materials were investigated in this manner, specifically carbon, silicon, silicon carbide, silicon nitride, and ruthenium. After capping the reflectance was measured again using the ALS beamline 6.3.2 reflectometer.

A reflectance map measured at EUV wavelengths (13.4nm) of one of the repair samples is shown in Figure 9. Figure 9(a) shows a reflectance map of a crater that is not protected by a capping layer. A lineout on the right of Figure 9(a) shows a maximum reflectance variation, ΔR_{max}, of 7.4%, which is the constant along the length of the crater. We repeated this experiment three times and obtained an average maximum reflectance variation of 7%.

Figure 9 (b) shows the EUV reflectivity of a crater that was capped with carbon prior to exposure to air. The sputter target was located near the top of the picture so that the capping layer thickness is thickest at the top of the picture and thinnest near the bottom. The lineouts on the right are profiles of the reflectivity across the crater at different distances from the target and, therefore, through different thickness' of capping layer material. The capping layer thickness as a function of the distance from the sputter target was estimated by sputtering carbon onto an unperturbed (crater-free) region of the multilayer and measuring the spatial dependence of the reflectance. At the position of the lineouts shown in Figure 9(b) the carbon capping layer thickness was estimated to be 3nm, 2nm, 1.7nm, and 1nm respectively from top to bottom.

This procedure was repeated for different capping layer materials. A summary of the results is shown in Figure 10, which details the maximum reflectance loss measured at the optimum capping layer thickness for the different capping layer materials, the optimum capping layer thickness being the profile in which the reflectivity variation across the crater was minimized. We also included error bars indicating 90% confidence intervals for ΔR_{max}. These experiments with in-situ ion beam sputtering indicate that both carbon and silicon carbide are the most promising materials of the capping layer materials investigated because they lead to the smallest maximum reflectance variation over the repair zone ΔR_{max}, of 3%. Note, however, that other deposition techniques might lead to different films and therefore different results.

3 An integrated approach to repairing defects in EUV mask blanks

We now turn to the issue of the increase in yield that can be expected through the use of defect repair techniques. The motivation behind investigating this is one of economic viability: it is all very well to propose a practical technique for defect repair, but it will not provide a practical or economic solution to the problem of defects in EUV masks unless there is an appreciable increase in the yield of useable mask blanks. In this paper we have described a technique for the repair of defects on the surface or in the upper layers of the multilayer stack, and in a previous paper we described a complementary technique for the repair of defects at or near the base of the multilayer[2]. Combining these two techniques with an appropriate multilayer coating process potentially enables the repair of any defect on an unpatterned mask blank.

The proportion of defects that can be repaired depends on both where the defects occur in the multilayer coating and the defect locations for which each technique can be successfully applied. Turning first to the question of defects location, defects can be nucleated in several distinct ways during the blank manufacture process:

1. Defects from handling will be introduced either before or after multilayer deposition and will manifest themselves as either phase defects if they are located on the substrate or as amplitude defects if they are on the surface;
2. Defects in the substrate such as pits, bumps and scratches from the polishing process will nucleate defects at the bottom of the multilayer stack and will manifest themselves as phase defects;
3. Defects introduced during the multilayer coating process can occur in any layer. Experience suggests that ion beam sputter systems clean up slightly during use, thus one could expect that the defect density may decrease slightly during the coating process.

The actual number and relative proportion of defects in each category will depend on handling, substrate polishing techniques and the cleanliness of the ion beam deposition system. The relative contributions of each of these to the total defect density will differ for different systems and must therefore be determined for each embodiment of the blank manufacture process.

Ideally the multilayer coating process itself should be defect free, in which case all defects are nucleated at either the top or bottom of the multilayer stack and there are no defects within the multilayer stack itself. In this case all defects are amenable to repair using either the phase or amplitude repair techniques provided the multilayer is made to be at least 40 bilayers thick.

However if the multilayer deposition process can not be made perfectly defect free a small proportion of defects will be nucleated within the multilayer stack itself, in which case it is necessary to determine what proportion of defects nucleated during multilayer deposition can be

repaired. The repairability criterion for amplitude (ion beam) repair has been discussed above: a defect can be repaired provided that more than 35 bi-layers must remain following the repair, to preserve multilayer reflectivity, whilst no more than 20 bilayers can be removed so as to preserve image placement.

For phase defect (e-beam) repair the repair full modelling of the repair process is computationally intensive, involving electron beam, thermal, electromagnetic and aerial image modelling, the details of which are beyond the scope of this discussion. Calculations reported elsewhere[8] indicate that a 50nm defect must be buried beneath at least 40 bilayers in order to be repairable using the phase defect repair technique, whilst a 120nm defect can be repaired if it is buried under at least 80 bilayers. The key variable for phase defect repair is the magnitude of the perturbation in the multilayer stack before and after repair and the maximum allowable CD variation in the printed image. The surface bump height is indicative of the layer disturbance caused by the defect nucleus, so we make the simplifying assumption that a defect unprintable if the bump height at the surface is less than 1nm and the defect is buried at least 35 layers below the surface. A defect is considered to be repairable using phase defect repair if the surface bump height is less than 4nm and there are at least 30 Mo/Si bilayers on top of the defect. These estimates of printability criterion are based on aerial image calculations in which the maximum acceptable CD variation for an isolated defect is pegged at 20%, in accordance with criteria described elsewhere[9]. We calculated the surface bump height for defects of different sizes and locations assuming an ion-assisted ion-beam deposition process designed to enhance the particle smoothing properties of the multilayer coating[10,11,12] and applied the criterion for defect printability described above to produce printability and repairability curves shown in Figure 11(a) and Figure 11(c). The selection of appropriate limiting values is subject to some discretion

and is process-dependent, however for the purposes of this analysis we suggest this as a reasonable criterion of the type defect locations repairable using each technique for a given deposition process.

Combining these two strategies together we have an integrated repair process which can address defects nucleated more than 40 bilayers beneath the surface with phase defect repair, whilst amplitude defect repair can be used for defects nucleated at least 35 bilayers from the substrate and less than 40 bilayers from the surface.

Having identified the classes of printable and repairable defects, we now turn to parametrisation of the defect distribution through the multilayer stack. For a given deposition process the proportion of defects within the multilayer bulk that can be repaired, and therefore the process yield, depends on both the defect size density distribution for the particular process and the number of bilayers deposited on the mask blank. Consider a multilayer coating that has a statistical distribution of defect nucleus sizes through the multilayer stack, and let the defect distribution be parameterised in terms of defect nucleus size R and position in the multilayer stack z. To take account of substrate and surface defects we let defects on the substrate occur in layer $z = 0$ and defects on the surface occur in layer $z = n$, where n is the number of bi-layers in the multilayer coating. The total number of defects on the mask is therefore simply the total of all defects of all sizes in all layers.

The size distribution of defects through the multilayer depends on both the coating process and handling protocols, and will have to be determined for each different coating system. However for illustrative purposes we choose the known size distribution from a low-defect deposition process with a total added defect density of less than 0.05 defects/cm^2, where the defect density was observed to vary with size according to the relation

$$N(d) \propto 0.02 d^{-0.54}$$

where $N(d)$ is the number of defects per cm^2 greater than a given size d. The statistical distribution of these defects through the multilayer stack is not known, so for the purposes of this discussion we assume two illustrative cases: (1) where all the defects are on either the surface or substrate, and (2) where all the defects are distributed uniformly through the multilayer coating. The resultant printable defect densities before and after repair are shown in Figure 12 for multilayers of different thickness', where care has been taken to ensure that the number of defects added per bi-layer is kept constant to take account of the fact depositing more layers may introduce more defects into the coating. The key question for determining the improvement in yield through the use of defect repair is one of identifying the proportion of printable defects that can be rendered unprintable through the use of defect repair techniques.

Adopting the previously described limits on the size and location of defects that can be repaired using both the amplitude and phase defect repair techniques, and the observation that certain classes of defect are not intrinsically printable, we can now calculate the improvement in yield resulting from the use of defect repair strategies. We do this using Monte-Carlo simulations in which defects of random sizes and locations are placed on hypothetical mask blanks with a quality area of 201cm^2, and then repaired using the techniques described above. The mask blank yield is defined as the fraction of mask blanks without any printable defects. For each set of simulation parameters, we performed calculations for 50,000 mask blanks to gain a good statistical description of the data set. We assumed that the density of defects located at the top and bottom surface of the multilayer was 0.01/cm^2 each, and that the remaining defects

were homogenously distributed through the multilayer stack, with a defect density of $2x10^{-4}/cm^2$ per Mo/Si bilayer and a total density of defects smaller than 20nm of $0.03/cm^2$.

Figure 12 shows the yield of mask blanks with 50 Mo/Si bilayers as a function of defect-repair treatment, as obtained by Monte-Carlo simulations. The calculations were performed for three different distributions of the defects through the mask blank: In the first set of simulations, we assumed that 1/3 of the defects are located at the top surface of the multilayer, and 1/3 of the defects are located at the bottom surface of the multilayer. The remaining 1/3 of the defects are distributed uniformly throughout the bulk of the multilayer. In the second set of simulations, we assumed that the bulk of the multilayer is defect-free, and that 1/2 of the multilayer are present on the top and bottom multilayer surface, respectively. In the third set of simulations, we assumed that all the defects are uniformly distributed through the multilayer stack.

The results of our Monte-Carlo simulations of the yield improvement due to defect repair, as shown in Figure 12 clearly demonstrate that both amplitude and phase defect repair have the potential of significantly reducing the number of yield-limiting defects. We found that this conclusion holds true even for very different distributions of defects through the mask blank. The simulations also show that the yield improvement due to the combined application of amplitude- and phase-defect repair exceeds the simple sum of the yield improvements of amplitude- and phase-defect repair alone. This synergetic effect is due to the fact that amplitude-defect repair is aimed at repairing defects located toward the top surface of the multilayer, whereas phase-defect repair is aimed at repairing defects located toward the bottom of the multilayer stack, and that both techniques applied together potentially address defects though the full multilayer stack.

The number of bilayers deposited in the multilayer stack is an independent variable in these simulations, so we investigated the effect of varying the number of layer pairs on mask blank yield. The result is shown in Figure 13, which shows the yield of mask blanks with and without repair as a function of number of Mo/Si bilayers in the multilayer. Inspection of Figure 13 yields an interesting result, in which the printable defect density actually decreases as the number of bilayers is increased. With repair it is actually advantageous to increase the number of bilayers deposited on the mask blank as this increases the proportion of defects within the multilayer bulk that can be addressed using defect repair. For 40 to 70 bilayers, the yield of mask blanks after repair increases with increasing number of bilayers since amplitude-defect repair is able to repair defects that are located deeper into the multilayer. The additional number of defects due to the deposition of more bilayers is small. However, restrictions on image displacement limits the maximum number of bilayers that can be removed during amplitude-defect repair, and amplitude-defect repair stagnates eventually. Increasing the number of bilayers beyond 70 will then lead to a slow degradation of yield since the deposition of additional bilayers adds more defects. In summary, there is an optimum multilayer thickness that leads to a maximum yield improvement using amplitude- and phase-defect repair.

We therefore have the somewhat counter-intuitive result that a coating process that adds defects actually benefits from the deposition of additional multilayer material when combined with successful multilayer defect repair strategy. A similar result is observed if the coating process is essentially defect free – increasing the number of bilayers increases the number of defects accessible to the repair techniques, thus the printable defect density after repair actually decreases as more bilayers included in the multilayer.

4 Conclusions

In this paper we have presented a practical technique for repairing amplitude defects in multilayer coated EUVL mask blanks that involves local removal of the upper layers of the multilayer stack to produce a smooth, shallow and slowly varying crater in the multilayer surface. The repair method removes the defective region of the multilayer and substantially restores the multilayer reflectivity in the repaired region whilst introducing only a small phase shift over the repaired area that will not print within the process window of the printing tool. It was shown from theoretical arguments that the repair site will not be a phase defect if the slope of the crater walls is sufficiently gentle and the amplitude modulation within the repair zone is sufficiently small.

We have performed preliminary experiments to investigate the feasibility of this technique and observed a reflectivity drop in the repaired region of 7%, a value that is consistent with layer removal plus an additional amount consistent with the known reflectivity degradation of exposed Mo layers. To counter the reflectivity loss we applied capping layers to the repair region prior to exposure to air whilst the sample is still in vaccum using in-situ ion beam sputtering. Several candidate capping layer materials were experimentally investigated, with Carbon and Silicon Nitride providing the best performance of the materials studies, giving a reflectivity drop in the repair region of 3-4%, a significant improvement over the 7% reflectivity drop observed without the use of any capping layer.

The yield improvement through use of defect repair was estimated using Monte-Carlo techniques, defined as the fraction of mask blanks without any printable defects. Through the application of defect repair it was possible to increase the yield from 32% without defect repair to 87% if both phase and amplitude repair strategies are employed, which is a significant

improvement. Furthermore, calculation of the yield as a function of coating thickness, as measured by the number of bilayers in the multilayer stack, gives the somewhat counter-intuitive result that for a coating process that adds defects, the yield actually increases as more layers are added to the coating thickness, reaching a maximum when the coating is 70 bilayers thick. It is therefore possible to adjust the number of layers deposited in the multilayer coating so as to optimise the mask blank yield if defect repair strategies are employed.

5 Acknowledgments

This work was performed under the auspices of the US Department of Energy by the University of California, Lawrence Livermore National Laboratory under contract No. W-7405-Eng-48. Funding was provided by the Extreme Ultraviolet Limited Liability Company (EUV LLC) under a Cooperative Research and Development Agreement, and by International Sematech under a Work-for-Others Agreement.

6 References

[1] T.Liang et.al. “Progress in EUV mask repair using a focussed ion beam” (2000) **18(6)** J.Vac.Sci.Ttechnol.B. 3216

[2] P.B.Mirkarimi, D.G.Stearns, S.L.Baker, J.W.Elmer, D.W.Sweeney, E.M.Gullikson "Methods for repairing Mo/Si multilayer thin film phase defects in reticles for extreme ultraviolet lithography’ (2002) **91** *J.Appl.Phys*. 81-89

[3] A.Barty, P.B.Mirkarimi, D.G.Stearns, D.Sweeney, H.N.Chapman, M.Clift, S.Hector and M.Yi EUVL mask blank repair” (2002) *Proc. SPIE*, Vol 4688, 385-394

[4] S.Hau-Riege, A.Barty, P.B.Mirkarimi, D.G.Stearns, H.Chapman, D.Sweeney, M.Clift, E.Gullikson and M.Yi ”Defect repair for extreme ultraviolet lithography (EUVL) mask blanks” (2003) *Proc. SPIE*, Vol. 5037, 331-338

[5] F.Zernike, “Phase contrast, a new method for the microscopic observation of transparent objects” (1942) **9** *Physica* 686-693.

[6] M.R.Teague “Image formation in terms of the transport equation” (1985) **11** *J.Opt.Soc.Am.A*. 2019.

[7] D.G.Stearns, D.W.Sweeney, P.B.Mirkarimi and H.N.Chapman “A method to repair localised amplitude defects in EUV lithography mask blanks” US Patent application CIL-10843

[8] E.M.Gullikson, C.Cerjan, D.G.Stearns, P.B.Mirkarimi and D.W.Sweeney "A practical approach for modelling EUVL mask defects" (2001) **20** *J.Vac.Sci.Technol.* 81-86

[9] A.Stivers and E.Tejnil: "Dependence of mask defect printability and printability criteria on lithography process resolution" (2002) Proc.SPIE Vol. 4562, 122-129

[10] P.B.Mirkarimi, E.A.Spiller, D.G.Stearns, V.Sperry, S.L.Baker: "An ion-assisted Mo/Si deposition process for planarising reticle substrates for extreme ultraviolet lithography" (2001) **37** *J.Quant.Elec*. 1514-1516

[11] P.B.Mirkarimi, E.Spiller, S.L.Baker, V.Sperry and D.G.Stearns "Developing a viable multilayer coating process for EUVL reticles" *Journal of Microlithography, Microfabrication and Microsystems (JM3)* (in press)

[12] D.G. Stearns, P.B. Mirkarimi, and E.Spiller, "Localized defects in EUV multilayer coatings" *Thin Solid Films* (in press)

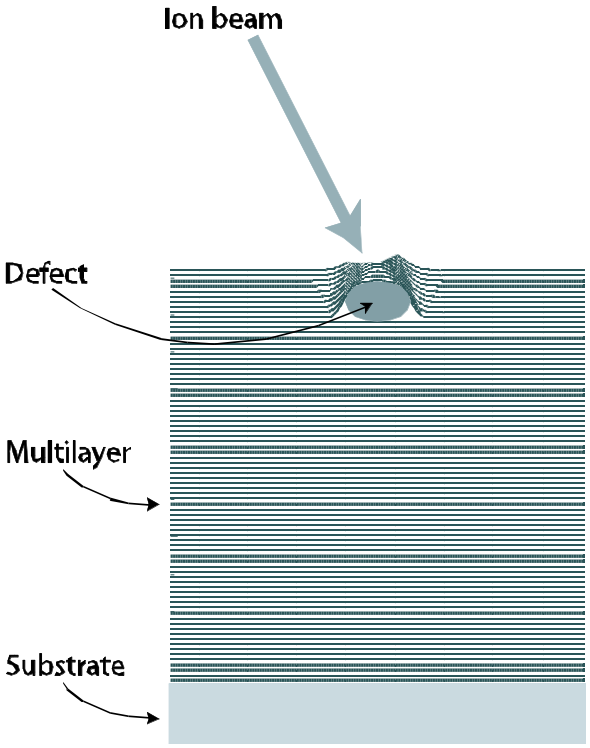

(a) Amplitude defect removal using a focussed ion beam.

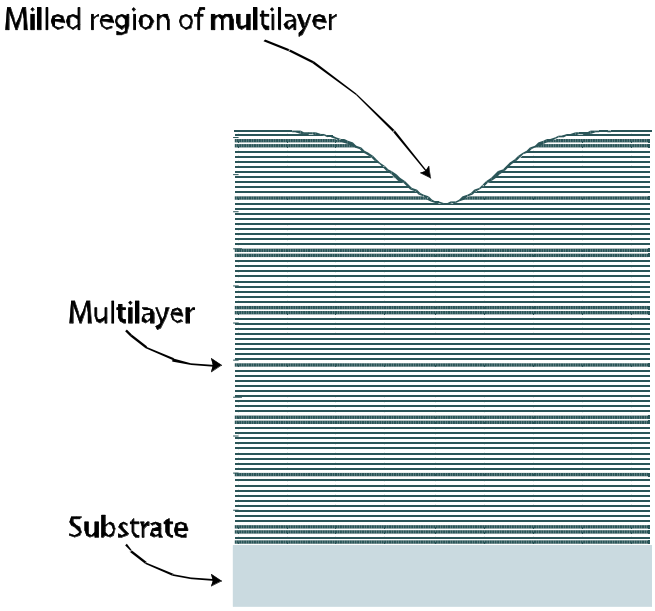

(b) Amplitude defect after repair – a small crater remains in the multilayer.

Figure 1

Amplitude repair technique

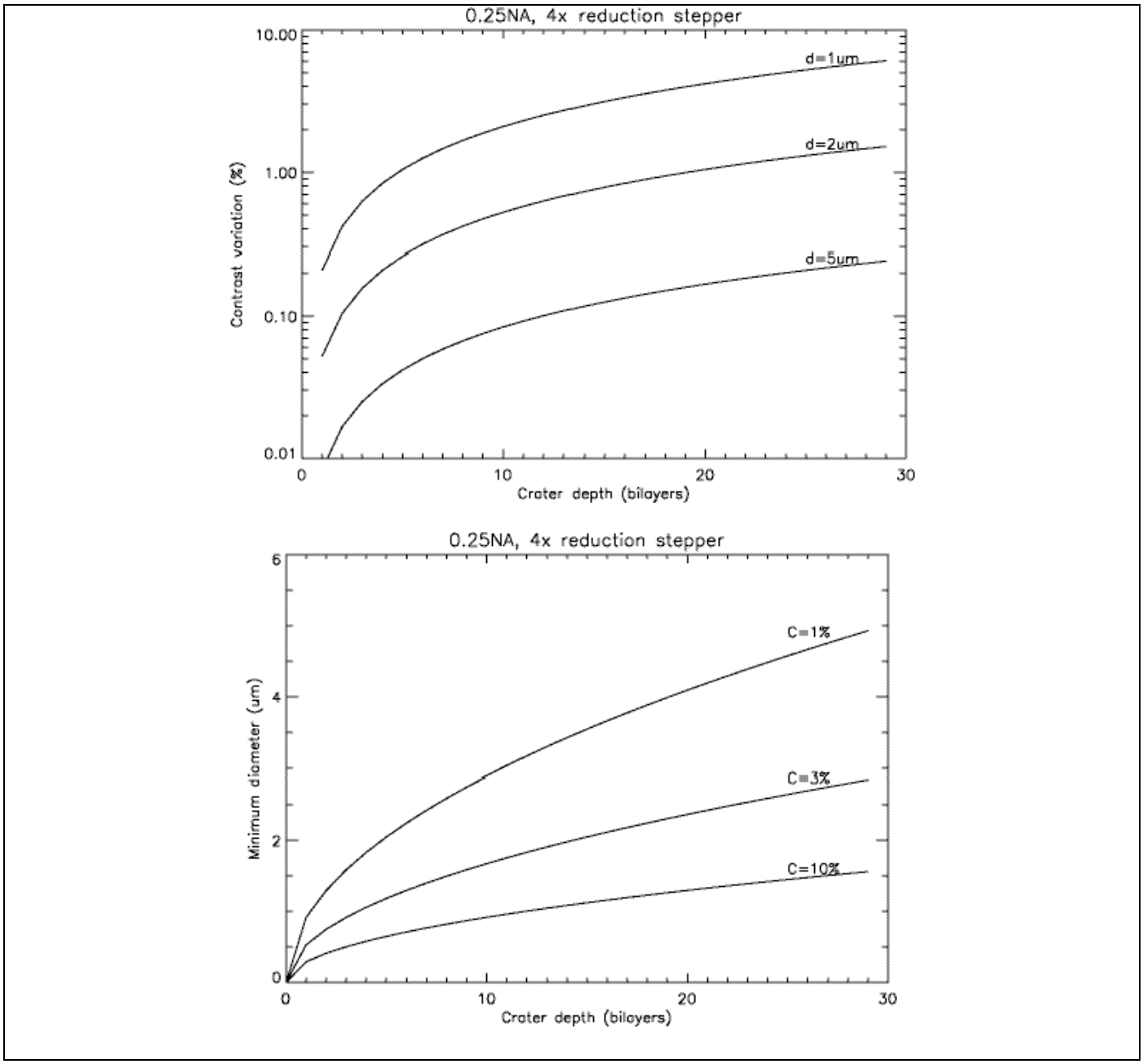

Figure 2

Minimum crater diameter as a function of depth and contrast

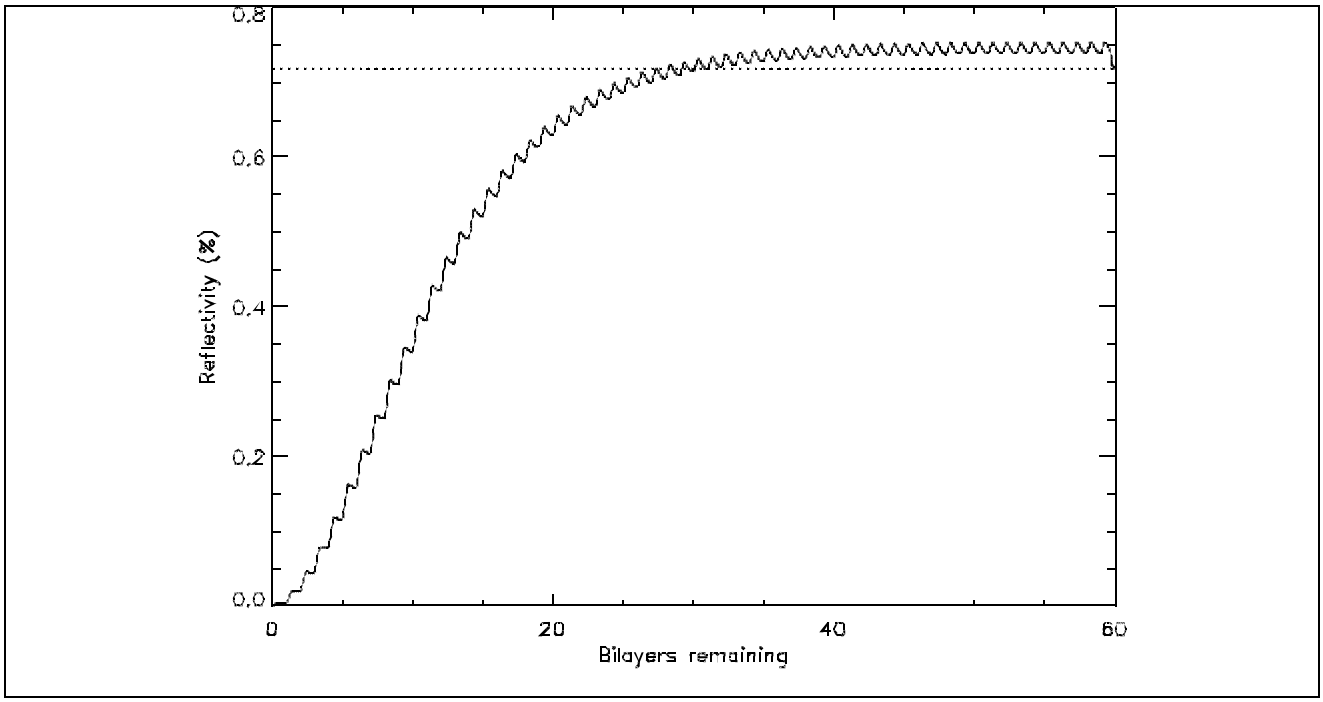

Figure 3

Reflectivity of a Mo/Si multilayer as a function of number of layers.

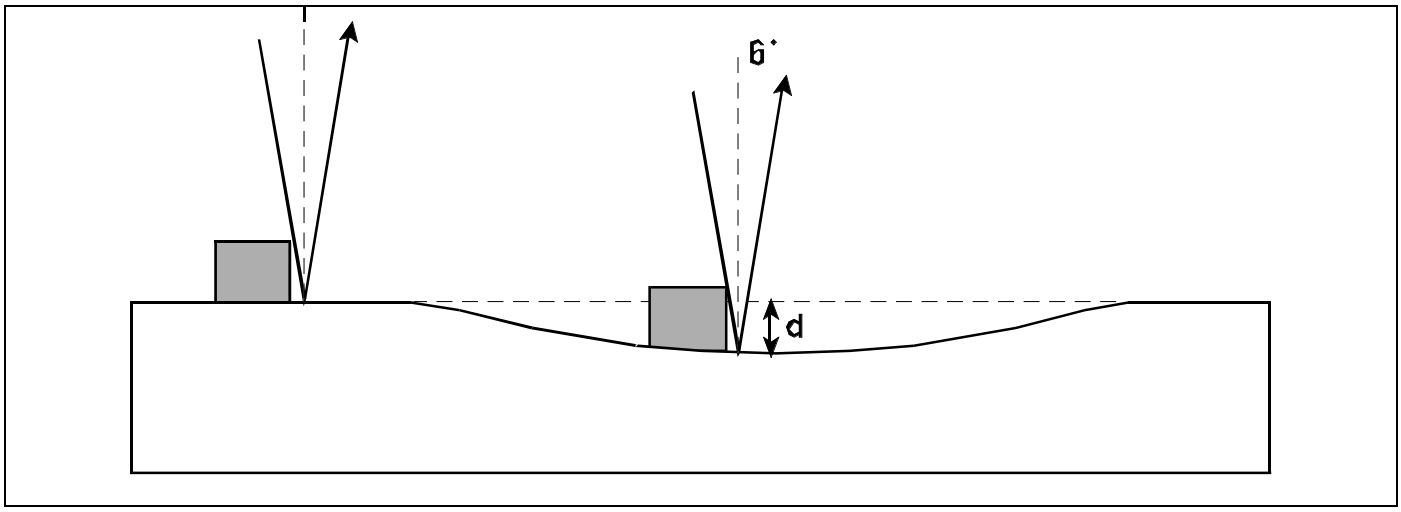

Figure 4

Image placement error caused when the pattern is placed within the crater.

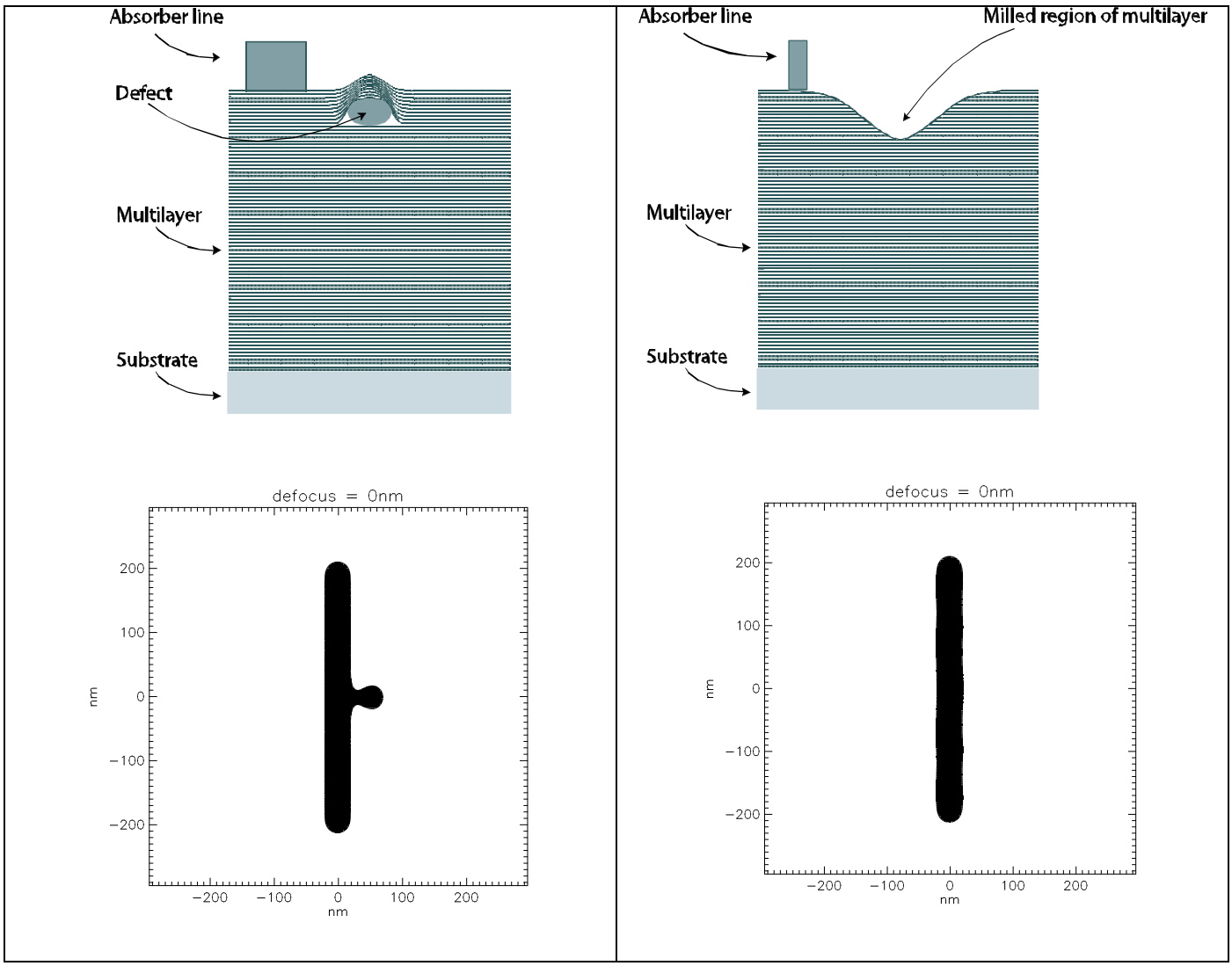

Figure 5

Aerial image calculation before (left) and after (right) amplitude defect repair.

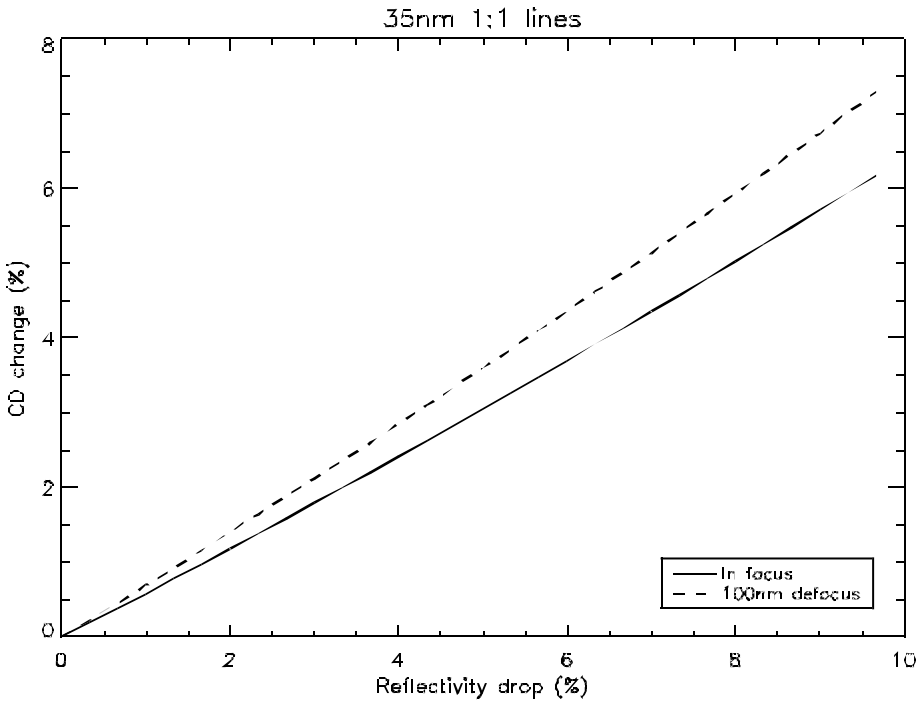

Figure 6

CD change of the printed line as a function of reflectivity drop inside the cratered region.

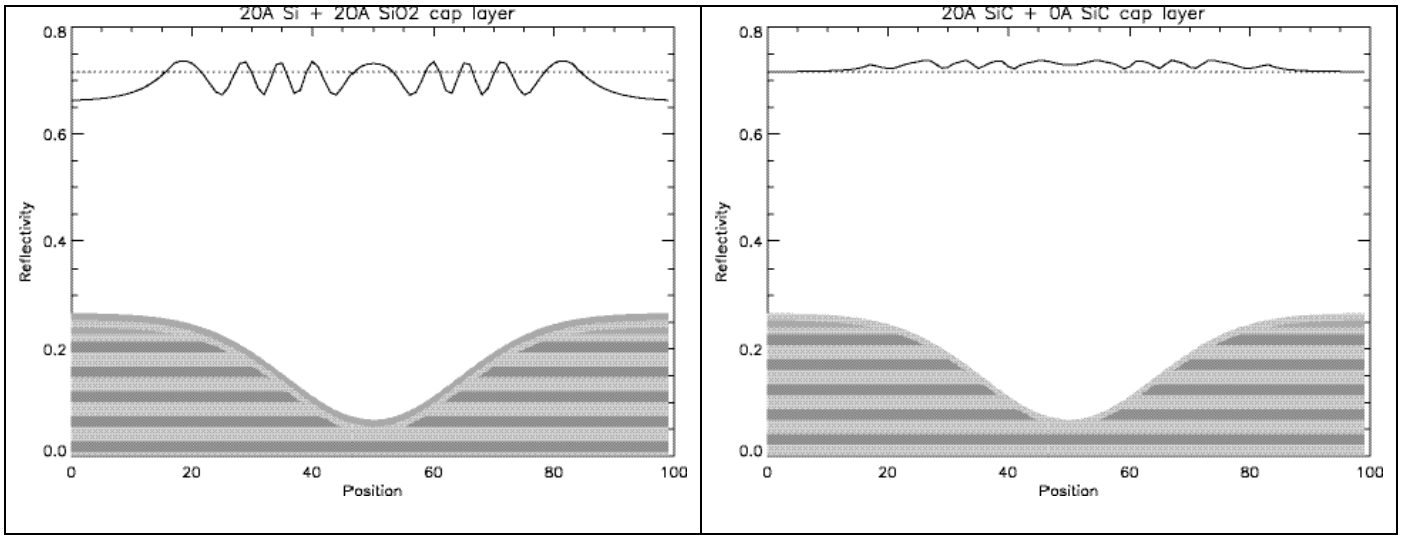

Figure 7

Predicted reflectivity across crater for two different capping layers

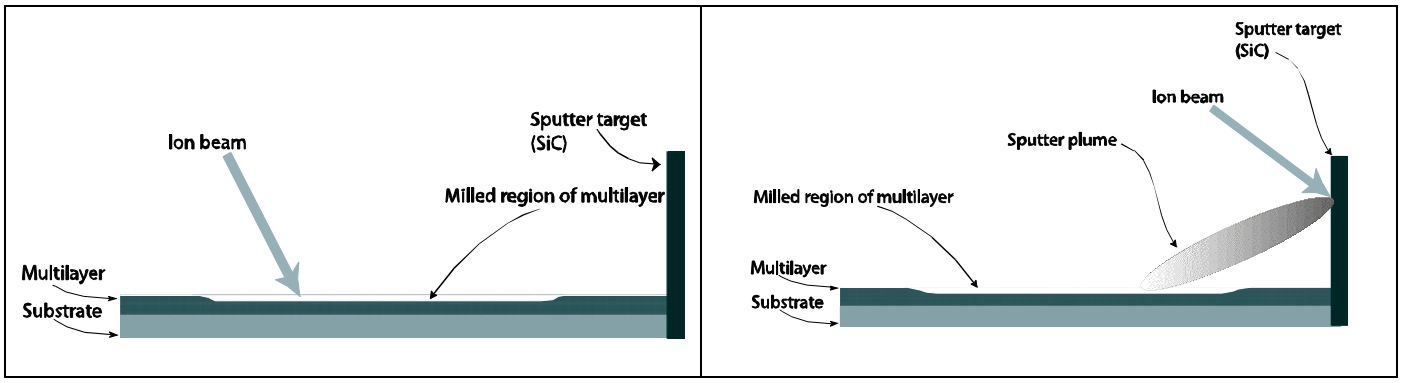

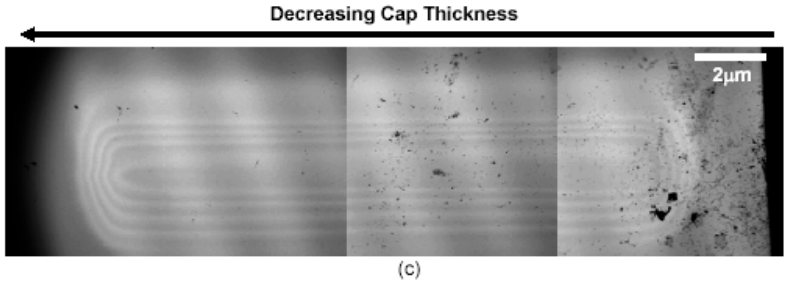

Figure 8

In-situ ion beam sputtering is used to apply a localised capping layer to the repaired region. (a) Argon ion beam sputtering is used to create a crater in the multilayer. The crater is the repair zone. (b) A capping layer is sputtered from the target onto the repair zone. (c) A top-down optical microscope picture of the repair zone.

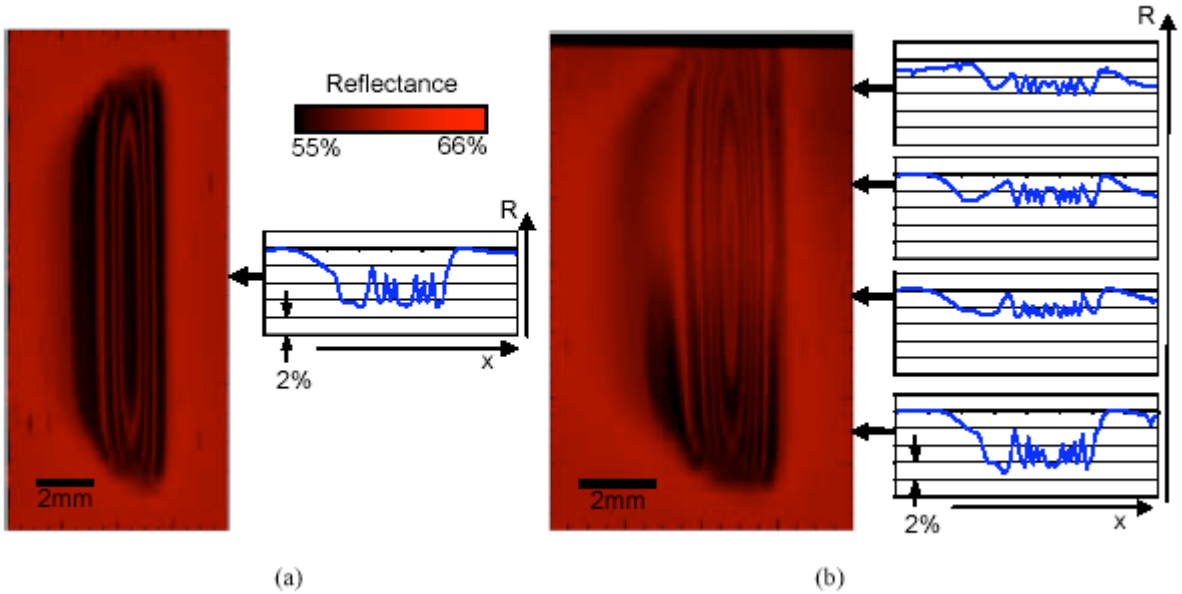

Figure 9

Reflectance maps (a) without capping layer and (b) with carbon capping layer. Also shown are lineouts of the reflectance at different locations along the crater. The maximum variation in reflectance, .R_{max}, is 7.4% for case (a), and, top-down, 4.0%, 3.7%, 3.0%, and 7.2% for case (b).

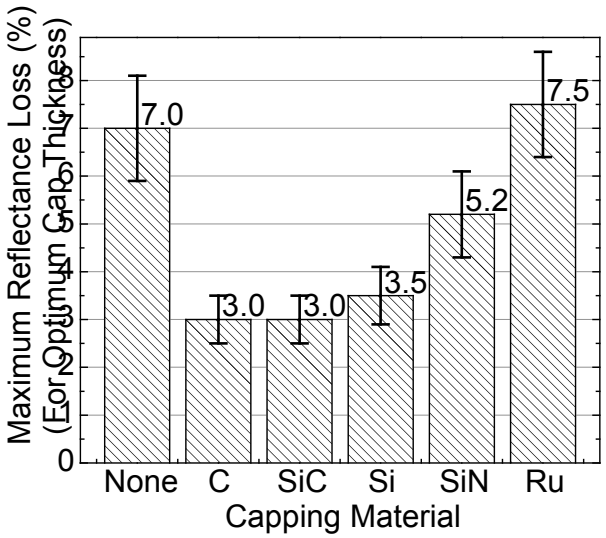

Figure 10

Measured best-case reflectance loss for uncoated craters and craters coated with C, SiC, Si, SiN, and Ru, respectively. The error bars indicate 90% confidence intervals.

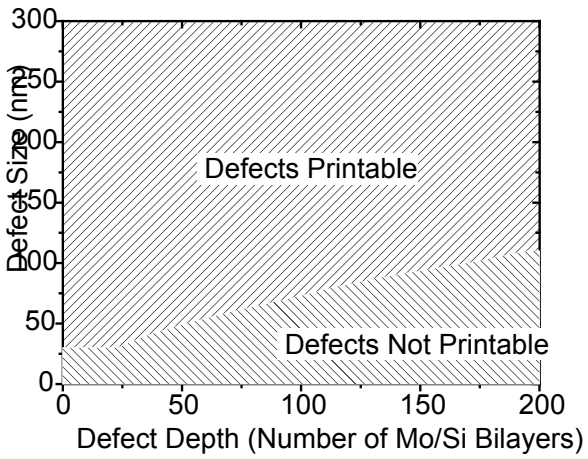
Defects Printable
Defects Not Printable
Defect Size (nm)
Defect Depth (Number of Mo/Si Bilayers)
0
50
100
150
200
250
300

(a)

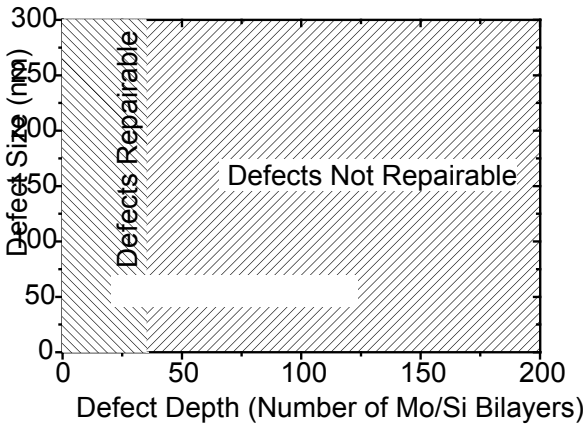
Amplitude Defect Repair
Defects Repairable
Defects Not Repairable
Defect Size (nm)
Defect Depth (Number of Mo/Si Bilayers)
0
50
100
150
200
250
300

(b)

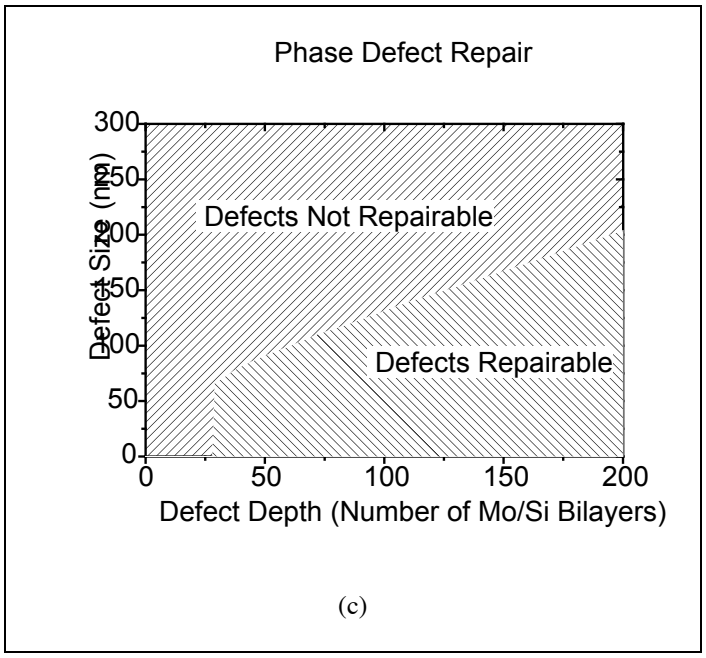
Phase Defect Repair
Defect Size (nm)
300
250
200
150
100
50
0
Defects Not Repairable
Defects Repairable
0
50
100
150
200
Defect Depth (Number of Mo/Si Bilayers)

(c)

Figure 11

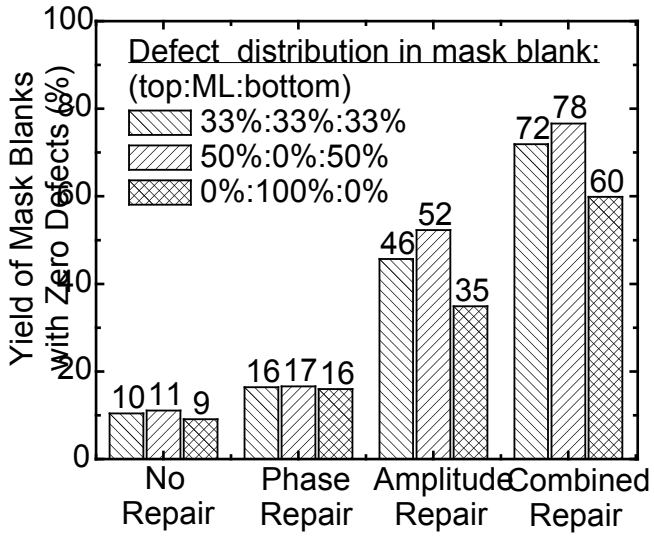

Figure 12

Improvement in yield with repair strategies.

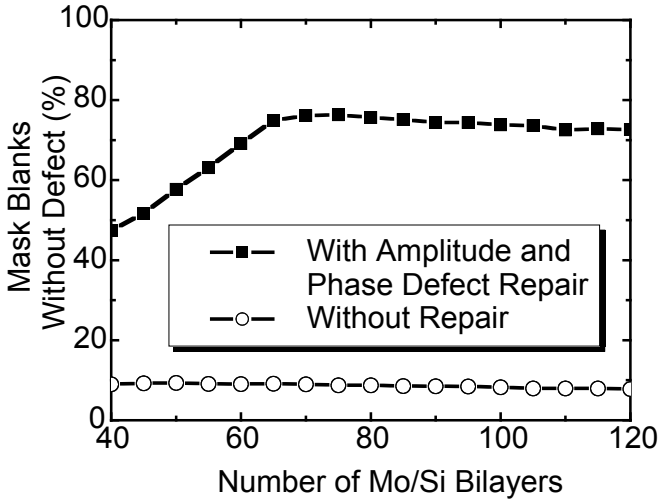

Figure 13

Dependence of yield on the number of multilayers deposited on the mask blank.